Electronic Supplementary Material

# Towards Efficient and Stable Organic Solar Cells: Fixing the Morphology Problem in Block Copolymer Active Layer with Synergistic Strategies Supported by Interpretable Machine Learning

Yu Cui, [a] Qunping Fan, [a] Hao Feng, [b] Tao Li, [b] Dmitry Yu. Paraschuk, [c] Wei Ma, [a] and Han Yan *[a]

[a] State Key Laboratory for Mechanical Behavior of Materials, School of Materials Science and Engineering, Xi'an Jiaotong University, Xi'an 710049, China. E-mail: mseyanhan@xjtu.edu.cn.
[b] Center for Spintronics and Quantum Systems, State Key Laboratory for Mechanical Behavior of Materials, School of Materials Science and Engineering, Xi'an Jiaotong University, Xi'an 710049, China.
[c] Faculty of Physics, Lomonosov Moscow State University, Leninskie Gory 1/62, Moscow 119991, Russia.

# 1. Experimental section

**1.1 Materials**. PM6 and Y6 were purchased from Solarmer Materials Inc. N-DMBI and chloroform (CF) were purchased from Sigma-Aldrich. All chemicals were used as received without further purification.

**1.2 BHJ device fabrication.** N-DMBI were dissolved in chloroform solvent with different concentrations (0.1mg/mL, 0.01mg/mL, 0.001mg/mL) and stirred on a hot plate at room temperature. PM6:PYIT (16 mg/mL, D/A = 1:0.87), Y6 (15 mg/mL), and PM6-b-PYIT (15 mg/mL) were dissolved in CF and stirred on a hot plate at 50 °C for 2 hours. All the organic solar cells were fabricated in a conventional device structure of ITO/PEDOT:PSS/active layer/PDINO/Al. Blended solutions were spin-coated on the substrates to form 100 nm films. Then a thin PDINO layer (2 mg/mL in methanol, 3300 rpm for 30 s) was spin-coated on the active layer. Finally, 100 nm Ag was deposited at a vacuum level of < $4\times10^{-5}$ Pa. The typical device area (0.04 $cm^2$) was defined by a metal mask with aligned aperture.

**1.3 GIWAXS characterization.** GIWAXS measurements were performed at beamline 7.3.3 at the Advanced Light Source.[1] Samples were prepared on Si substrates using identical blend solutions as those used in devices. The 10 keV X-ray beam was incident at a grazing angle of 0.11°-0.15°, selected to maximize the scattering intensity from the samples. The scattered x-rays were detected using a Dectris Pilatus 2M photon counting detector. Crystal coherence lengths (CCLs) values of the materials were calculated using Scherrer equation:

$$\mathrm{CCLs} = \frac{2\pi K}{\Delta\ q}$$

$K$ (shape factor) = 0.9 and $\Delta\ q$ =full width half maximum (FWHM) of the scattering.

**1.4 DFT and TD-DFT calculation.** We apply density functional theory (DFT) and time-dependent density functional theory (TD-DFT) to study the interaction among PM6-b-PYIT, the PM6-block, the PYIT-block, Y6 and N-DMBI. All DFT calculations

in this work were performed using the ORCA 5.0.0 package.[2, 3] The gas-phase ground state geometry of the molecules was determined using the B3LYP/G D3 def2-TZVP method. We then used the M062X functional and base set with the polarizable continuum model (PCM) to perform all the remaining DFT calculations. The quantitative molecular surface analysis, non-covalent interaction (NCI) analysis and Mulliken charge population analysis were performed with the use of Multiwfn.[4]

**1.5 Molecular polarity index (MPI).** The electrostatic potential is directly determined by the charge distribution within a system; an uneven distribution of charge within a molecule manifests itself as a distinctive pattern of electrostatic potential across the molecular surface. Consequently, characterizing the features of the electrostatic potential distribution over a molecule's surface allows for quantification of the molecule's polarity. The molecular polarity index (MPI) is defined as follow:

$$\mathrm{MPI} = (1/A)\iint_S |V(\mathrm{r})|\, dS$$

Here, $V$ represents the molecular electrostatic potential, and integration is performed over the molecular surface S, with $A$ denoting the molecular surface area. A larger MPI signifies a greater overall polarity of the molecule. This is because the unevenness of the charge distribution serves as a manifestation of molecular polarity; the more pronounced the heterogeneity of the charge distribution, the more likely it is to produce highly positive or highly negative regions on the molecular surface, thereby resulting in a higher MPI value. The MPIs were calculated by Multiwfn.[4]

**1.6 Calculating the SCLC mobility.** The SCLC mobility (μ) was measured with the hole-only device structure of ITO/PEDOT:PSS/active layer/$MoO_3$/Al and electron-only device structure of ITO/ZnO/active layer/PFN-Br/Al. The thickness of all the active layers is maintained at approximately 100 nm. The values of SCLC mobility were obtained by fitting the current density-voltage curves according to

$$J = \frac{9\varepsilon_0\varepsilon_r\mu V^2}{8d^3}$$

where $\varepsilon_0$ is the permittivity of vacuum, $\varepsilon_r$ is the relative permittivity of the active layer and it is assumed to be 3.5 here.

**1.7 Kelvin Probe Force Microscopy:** KPFM images were obtained by a commercial SPM system (MFP3D, Oxford Instruments, USA). The surface potential was defined as $(\Phi_{tip} - \Phi_{sample})/e$. The conductive probe tip used in the measurements was Pt coated.

**1.8 Other measurements.** TM-AFM images were scanned by Bruker INNOVA. The J-V curves were performed in the $N_2$-filled glovebox under AM 1.5G (100 mW $cm^{-2}$) using an AAA solar simulator (SS-F5-3A, Enli Technology Co., Ltd.) calibrated with a standard photovoltaic cell equipped with KG5 filter. The EQE curves were measured by Solar Cell Spectral Response Measurement System QE-R3018 (Enli Technology Co., Ltd.) with calibrated light intensity by a standard Si photovoltaic cell. ESR spectra were tested on Bruker Biospin A300-9.5/12. ESR spectra were tested on Bruker Biospin A300-9.5/12. PL spectra were recorded by FLS980 spectrometer (Edinburgh Instruments, EI). The thickness of all thWWe PL samples maintained at approximately 100 nm.

**1.9 Machine Learning.** XGBoost ML algorithm was chosen because it uses parallelized processing, which can steadily improve the accuracy of the model. To avoid overfitting, grid search with 5-fold cross-validation (CV) was used to optimize the hyperparameters (Table S13). The dataset was split into a training dataset (70%) and a test dataset (30%). Root mean squared error (RMSE) and coefficient of determination ($r^2$) were used to check the performance of ML model:

$$\mathrm{MSE} = \sum_{i=1}^{m} \frac{1}{m}(x_i - y_i)^2$$

$$\mathrm{RMSE} = \sqrt{\mathrm{MSE}}$$

$$r^2 = 1 - \frac{\mathrm{MSE}}{Var(y)}$$

$x_i$ is the predicted value of the model, $y_i$ is the target variable and $Var(y)$ is the variance of the sample data. The coefficient of determination ($r^2$) indicates the prediction ability

of the model. Its value ranges between 0 and 1, and a value close to one indicates more prediction accuracy.

## 2. Supplementary figures

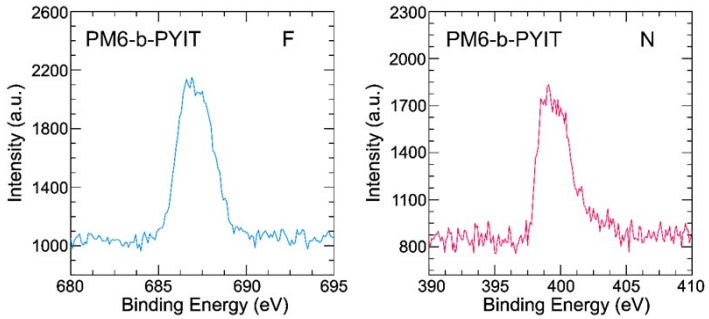


**Fig. S1.** XPS spectra: F 1s and N 1s spectrum of PM6-b-PYIT.

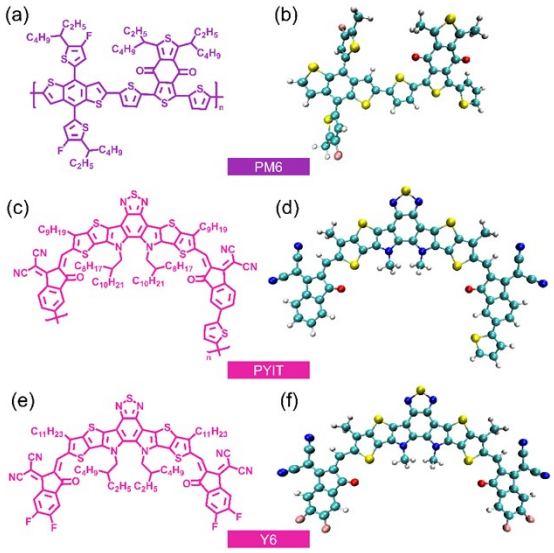


**Fig. S2.** Chemical structures and DFT calculated optimal geometries of (a)(b) PM6 (poly((4,8-bis(5-(2-ethylhexyl)-4-fluoro-2-thienyl)benzo[1,2-b:4,5-b']dithiophene-2,6-diyl)-2,5-thiophenediyl(5,7-bis(2-ethylhexyl)-4,8-dioxo-4H,8H-benzo[1,2-c:4,5-c']dithiophene-1,3-diyl)-2,5-thiophenediyl)), (c)(d) PYIT (poly[2,2'-((2Z,2'Z)-((12,13-bis(2-octyldodecyl)-3,9-diundecyl-12,13-dihydro-[1,2,5]thiadiazolo[3,4-e]thieno[2",3":4',5']thieno[2',3':4,5]pyrrolo[3,2-g]thieno[2',3':4,5]thieno[3,2-b]indole-2,10-diyl)bis(methanylylidene))bis(5,6-difluoro-3-oxo-2,3-dihydro-1H-indene-2,1-diylidene))dimalononitrile-co-2,5-thiophene]) and (e)(f) Y6 (2,2'-((2Z,2'Z)-((12,13-bis(2-ethylhexyl)-3,9-diundecyl-12,13-dihydro-[1,2,5]thiadiazolo[3,4-e]thieno[2",3":4',5']thieno[2',3':4,5]pyrrolo[3,2-g]thieno[2',3':4,5]thieno[3,2-b]indole-2,10-diyl)bis(methanylylidene))bis(5,6-difluoro-3-oxo-2,3-dihydro-1H-indene-2,1-diylidene))dimalononitrile)

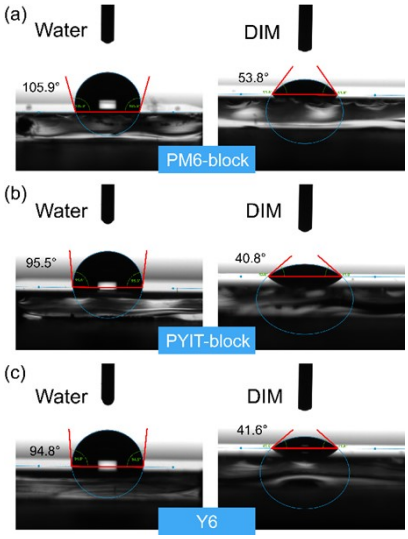


**Fig. S3.** The contact angle images of (a) PM6, (b) PYIT and (c) Y6.

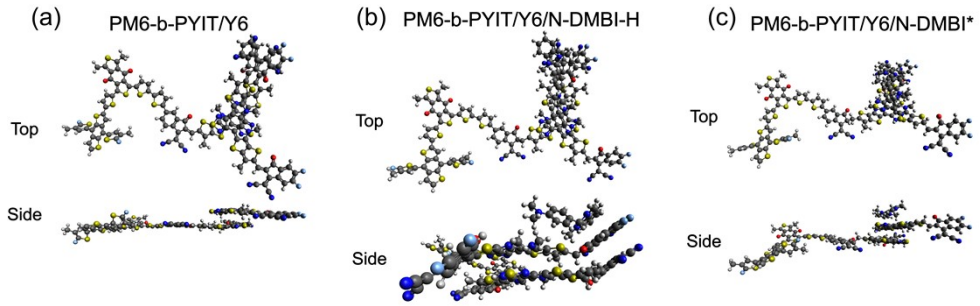


**Fig. S4.** DFT calculated optimal geometries of (a) PM6- PYIT unit/Y6, (b) PM6-PYIT unit/Y6/N-DMBI and (c) PM6- PYIT unit/Y6/N-DMBI* complexes.

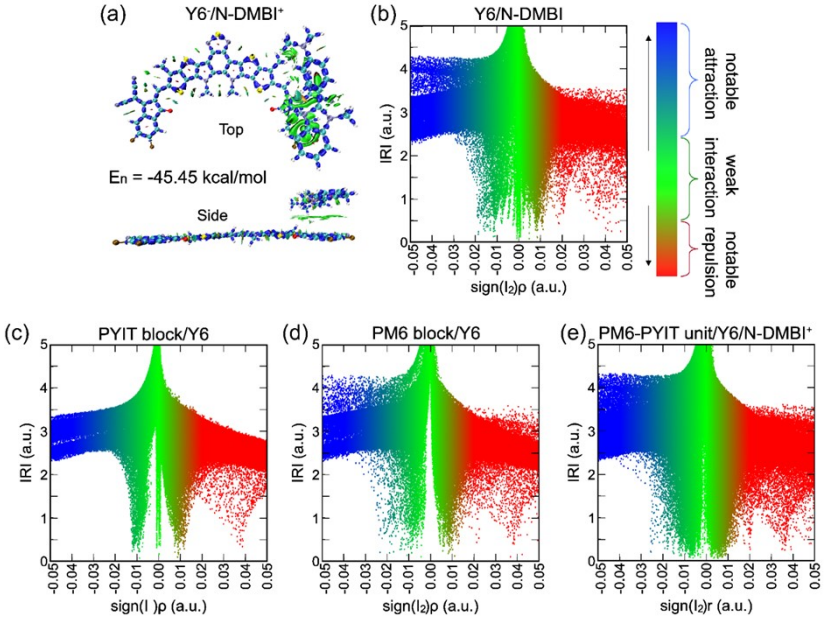


**Fig. S5.** (a) NCI calculated by reduced density gradient analysis of $Y6^{-}$/N-$DMBI^{+}$ complex and the respective non-covalent energy ($E_n$). The NCI interaction scatter plots of (b) $Y6^{-}$/N-$DMBI^{+}$, (c) PYIT block/Y6, (d) PM6 block/Y6 and (e) PM6-PYIT unit/$Y6^{-}$/N-$DMBI^{+}$ complex.

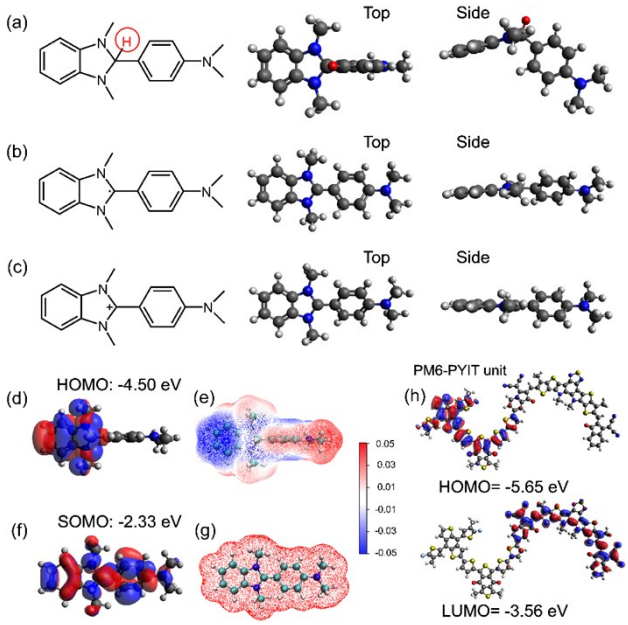


**Fig. S6.** Chemical fomula and optimized molecular geometries of the neutral (a) N-DMBI, (b) radical N-DMBI$^{*}$, and (c) cation N-DMBI$^{+}$. Pictorial representation and energies of (d) the HOMO of N-DMBI and (f) the SOMO of N-DMBI$^{*}$. Electrostatic potential (ESP) of (e) N-DMBI and (g) N-DMBI$^{+}$. (h) The calculated highest occupied molecular orbital (HOMO) and lowest unoccupied molecular orbital (LUMO) of PM6-PYIT unit.

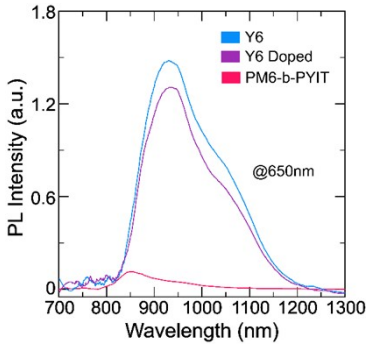


**Fig. S7.** PL spectra of the pristine Y6, Y6 doped by N-DMBI, and PM6-b-PYIT films. The PL intensities are normalized to the corresponding absorption of the films at the excitation wavelength of 650 nm.

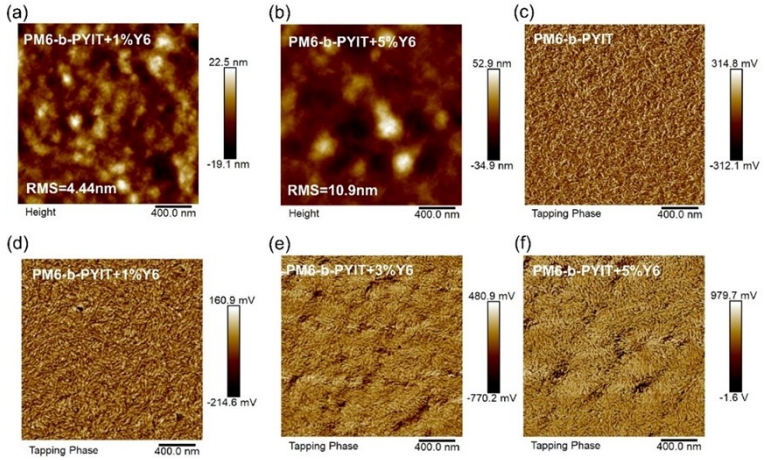


**Fig. S8.** AFM height image for (a) PM6-b-PYIT+1%Y6 and (b) PM6-b-PYIT+5%Y6 film. Phase images for (c) pristine PM6-b-PYIT, (d) PM6-b-PYIT+1%Y6, (e) PM6-b-PYIT+3%Y6 and (f) PM6-b-PYIT+5%Y6 films.

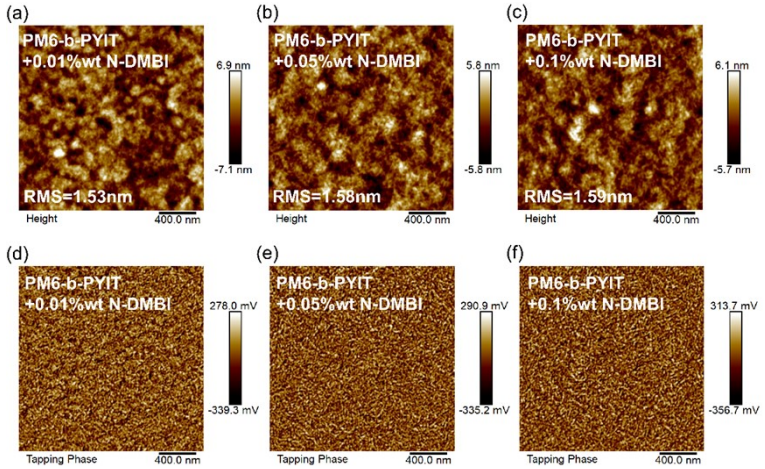


**Fig. S9.** AFM height and phase images for (a) and (d) PM6-b-PYIT+0.01%wt N-DMBI; (b) and (e) PM6-b-PYIT+0.05%wt N-DMBI; (c) and (f) PM6-b-PYIT+0.1%wt N-DMBI films.

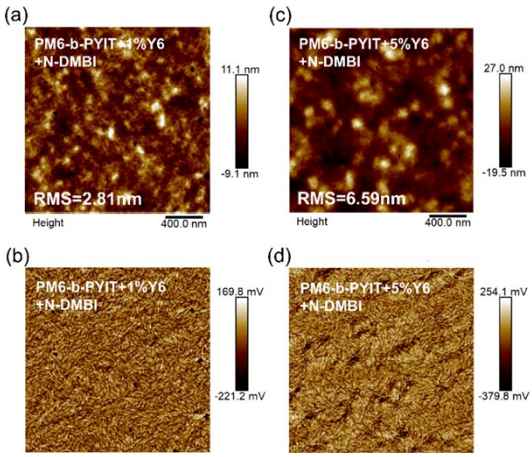


**Fig. S10.** AFM height and phase images for (a, b) PM6-b-PYIT+1%Y6 doped, (c, d) PM6-b-PYIT+5%Y6 doped films.

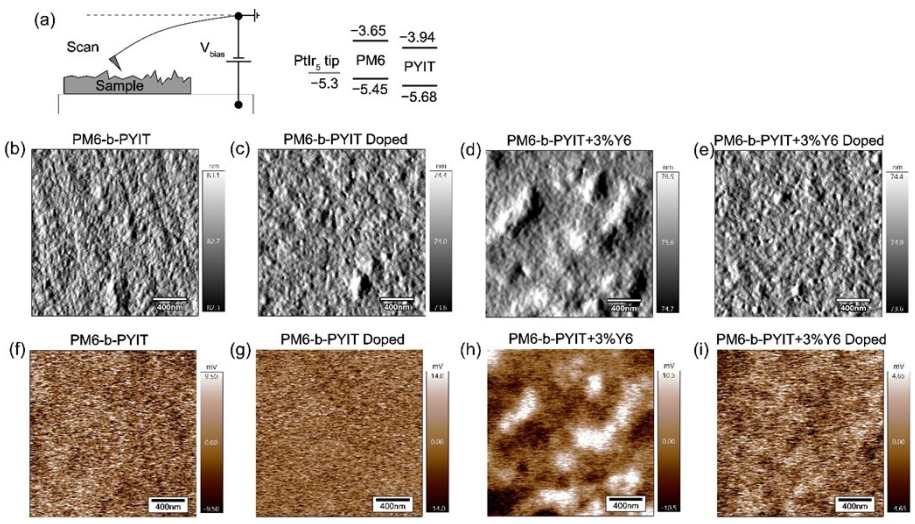


**Fig. S11.** (a) Schematic diagram of KPFM test. Height and KPFM image of (b, f) PM6-b-PYIT, (c, g) PM6-b-PYIT doped, (d, h) PM6-b-PYIT+3%Y6 and (e, i) PM6-b-PYIT+3%Y6 doped films, respectively.

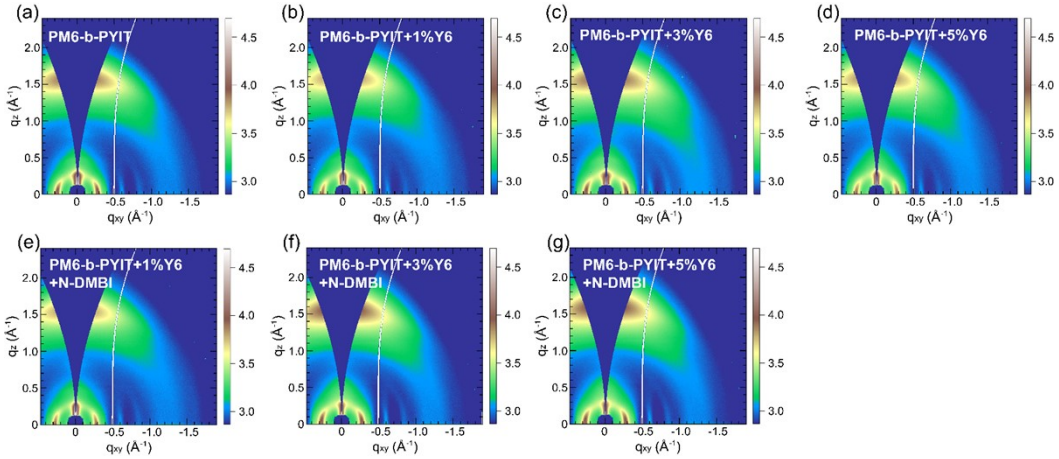


**Fig. S12.** 2D GIWAXS patterns for the films studied.

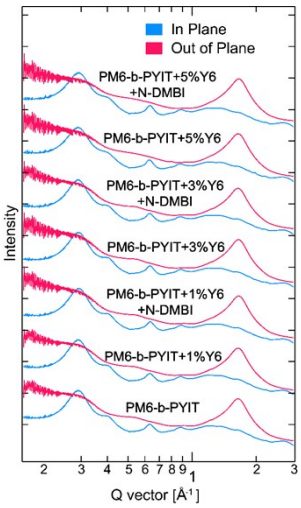


**Fig. S13.** Out-of-plane and in-plane 1D scattering profiles for the data from Fig. S13.

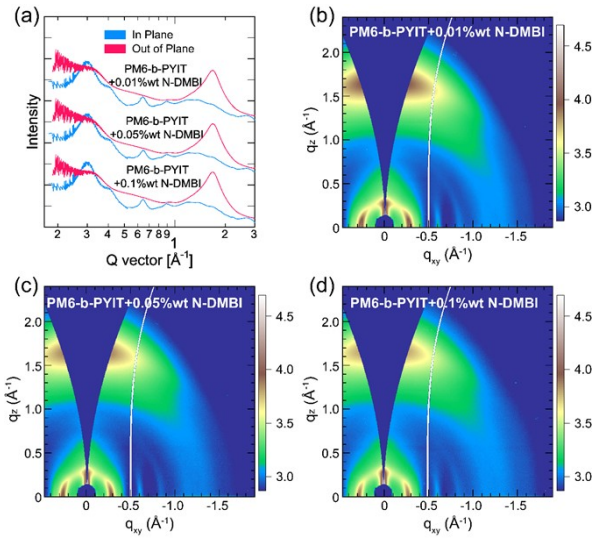


**Fig. S14.** (a) 1D scattering profiles of out-of-plane (OOP) and in-plane (IP) for PM6-b-PYIT+0.01%wt N-DMBI, PM6-b-PYIT+0.05%wt N-DMBI, and PM6-b-PYIT+0.1%wt N-DMBI films. (b-d) 2D GIWAXS patterns for their corresponding films.

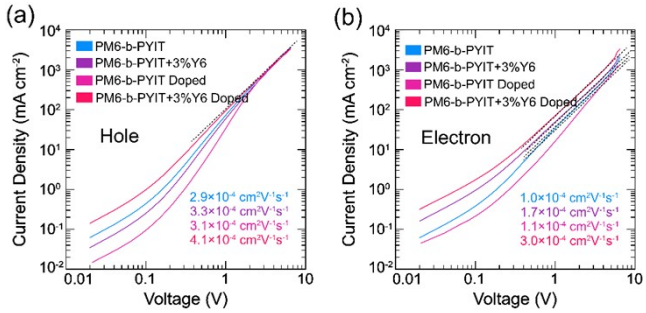


**Fig. S15.** (a) Hole-only and (b) electron-only charge transport curves of the pristine PM6-b-PYIT, PM6-b-PYIT+3%Y6, PM6-b-PYIT doped, and PM6-b-PYIT+3%Y6 doped devices.

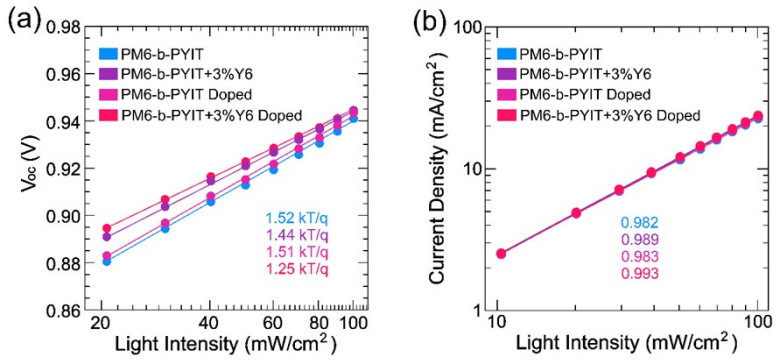


**Fig. S16.** $V_{OC}$ and $J_{SC}$ as a function of the light intensity.

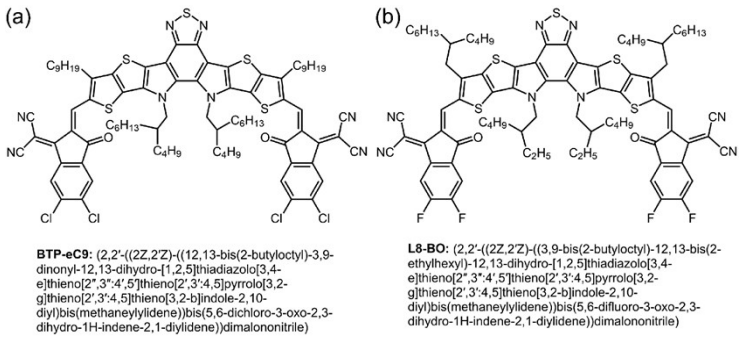


**Fig. S17.** Chemical structures and full names of (a) BTP-eC9 and (b) L8-BO.

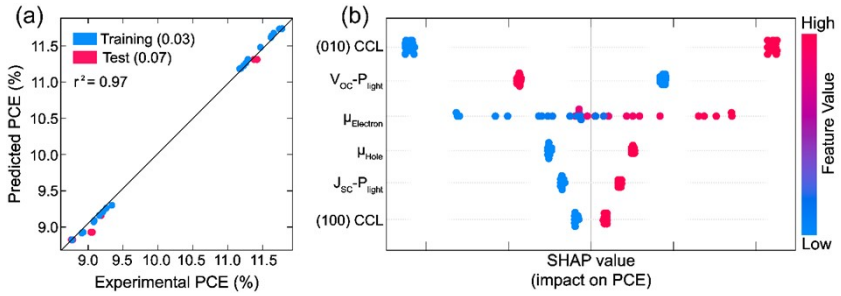


**Fig. S18.** (a) Predicted PCE by machine learning versus the experimental PCE. (b) Illustration of features contributing to photovoltaic performances by SHAP values. The relative contributions of morphology and charge transport/recombination parameters for PCE.

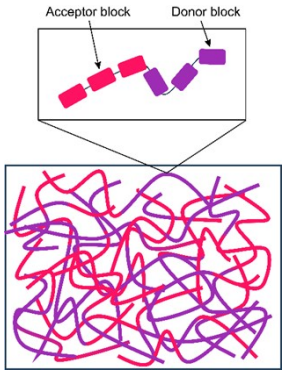


**Fig. S19.** Schematic of the unoptimized BCP morphology.

## 3. Supplementary tables

**Table S1.** The elemental analysis data of the block copolymer PM6-b-PYIT.

| | Element | Mass Fraction (%) | Atomic Fraction (%) |
|---|---|---|---|
| PM6-b-PYIT | N | 71.34 | 77.31 |
| | F | 28.66 | 22.69 |

**Table S2.** The photovoltaic performance parameters of OSCs based on PM6:PYIT (D:A = 1:0.87) and PM6-b-PYIT under the illumination of AM 1.5G, 100 mW $cm^{-2}$. [a]

| Photoactive Layer | $V_{OC}$ (V) | $J_{SC}$ (mA/$cm^2$) | FF (%) | PCE (%) |
|---|---|---|---|---|
| PM6:PYIT (D:A = 1:0.87) | 0.965 (0.961±0.002) | 24.1 (23.9±0.2) | 63.3 (61.0±0.7) | 14.6 (14.2±0.2) |
| PM6-b-PYIT | 0.943 (0.942±0.001) | 23.1 (23.0±0.1) | 60.7 (60.3±0.1) | 13.2 (12.9±0.2) |

[a] The parameters are obtained from 10 independent devices.

**Table S3.** Contact angle, surface energy and molecular polarity index of the used materials.

| Materials | $\Theta_{water}$ (°) | $\Theta_{DIM}$ (°) | Surface energy (mN/m) | Molecular polarity index (MPI) (kcal/mol) |
|---|---|---|---|---|
| PM6 block | 105.9 | 53.8 | 31.74 | 7.32 |
| PYIT block | 95.5 | 40.8 | 36.84 | 10.76 |
| Y6 | 94.8 | 41.6 | 37.87 | 11.51 |

**Table S4.** Enthalpy changes for the hydrogen atom removal reaction.

| Enthalpy Change | kcal/mol |
|---|---|
| $\Delta H_{H^*}$ (PM6-PYIT unit/N-DMBI) | 33.8 |
| $\Delta H_{H^*}$ (PM6-PYIT unit/Y6/N-DMBI) | 20.3 |

**Table S5.** Summary of the related energy quantities for the hydrogen atom removal reaction.

| Enthalpy | kcal/mol |
|---|---|
| $\Delta E_{H^*}$ (N-DMBI) | 83.4 |
| IP(N-DMBI$^*$) | 57.3 |
| $E_n$ (PM6-PYIT unit/N-DMBI) | -16.3 |
| $E_n$ (PM6-PYIT unit$^-$/N-DMBI$^+$) | -32.3 |
| $E_n$ (PM6-PYIT unit+Y6/N-DMBI) | -27.5 |
| $E_n$ (PM6-PYIT unit+Y6$^-$/N-DMBI$^+$) | -44.0 |

**Table S6.** Charge transfer amounts (CT) from the dopants to semiconductors.

| Mulliken charge population analysis | |
|---|---|
| | **Charge Transfer (*e*)** |
| PM6-b-PYIT/Y6/N-DMBI | 0.17 |
| PM6-b-PYIT/Y6/N-DMBI* | 0.98 |

**Table S7.** Calculated crystal coherence lengths (CCLs) from GIWAXS patterns.

| Conditions | (010) (Å) | | (11-1) (Å) | | (100) (Å) | |
|---|---|---|---|---|---|---|
| | FWHM | CCLs | FWHM | CCLs | FWHM | CCLs |
| PM6-b-PYIT | 0.306 | 18.46 | 0.064 | 88.71 | 0.131 | 50.33 |
| PM6-b-PYIT+1%Y6 | 0.284 | 19.89 | 0.052 | 108.99 | 0.056 | 100.18 |
| PM6-b-PYIT+1%Y6+0.05%wt N-DMBI | 0.243 | 23.29 | 0.047 | 120.18 | 0.050 | 112.47 |
| PM6-b-PYIT+3%Y6 | 0.282 | 20.02 | 0.051 | 111.76 | 0.049 | 114.11 |
| PM6-b-PYIT+3%Y6+0.05%wt N-DMBI | 0.265 | 21.36 | 0.052 | 109.09 | 0.048 | 116.88 |
| PM6-b-PYIT+5%Y6 | 0.269 | 21.06 | 0.056 | 101.12 | 0.056 | 101.40 |
| PM6-b-PYIT+5%Y6+0.05%wt N-DMBI | 0.269 | 19.08 | 0.052 | 107.94 | 0.053 | 105.72 |
| PM6-b-PYIT+0.01%wt N-DMBI | 0.308 | 18.35 | 0.065 | 86.95 | 0.111 | 50.92 |
| PM6-b-PYIT+0.05%wt N-DMBI | 0.308 | 18.35 | 0.064 | 88.31 | 0.113 | 50.02 |
| PM6-b-PYIT+0.1%wt N-DMBI | 0.310 | 18.23 | 0.066 | 85.64 | 0.113 | 50.02 |

**Table S8.** Photovoltaic performance of PM6-b-PYIT based OSCs fabricated by different amount of CN additives under the illumination of AM 1.5G, 100 mW $cm^{-2}$. [a]

| Condition | $V_{OC}$ (V) | $J_{SC}$ (mA/$cm^2$) | FF (%) | PCE (%) |
|---|---|---|---|---|
| PM6-b-PYIT | 0.940 (0.939±0.001) | 22.7 (22.4±0.2) | 59.0 (58.6±0.3) | 12.6 (12.4±0.1) |
| PM6-b-PYIT +0.5% CN | 0.945 (0.943±0.001) | 23.2 (23.0±0.2) | 59.5 (58.3±1.3) | 13.0 (12.5±0.3) |
| PM6-b-PYIT +1% CN | 0.943 (0.942±0.001) | 23.1 (23.0±0.1) | 60.7 (60.3±0.1) | 13.2 (12.9±0.2) |
| PM6-b-PYIT +2% CN | 0.944 (0.941±0.002) | 23.2 (23.1±0.1) | 58.5 (58.3±1.1) | 12.8 (12.4±0.3) |

[a] The parameters are obtained from 10 independent devices.

**Table S9.** Photovoltaic performance of OSCs fabricated by direct doping of PM6-b-PYIT with N-DMBI under the illumination of AM 1.5G, 100 mW $cm^{-2}$. [a]

| Condition | $V_{OC}$ (V) | $J_{SC}$ (mA/$cm^2$) | FF (%) | PCE (%) |
|---|---|---|---|---|
| PM6-b-PYIT +0.01%wt N-DMBI | 0.944 (0.942±0.002) | 22.8 (22.4±0.2) | 59.3 (57.9±0.9) | 12.8 (12.5±0.1) |
| PM6-b-PYIT +0.05%wt N-DMBI | 0.945 (0.943±0.001) | 22.9 (22.3±0.5) | 59.5 (57.3±1.3) | 12.9 (12.5±0.3) |
| PM6-b-PYIT +0.1%wt N-DMBI | 0.944 (0.941±0.002) | 22.5 (22.2±0.2) | 60.0 (58.0±1.1) | 12.8 (12.4±0.3) |

[a] The parameters are obtained from 10 independent devices.

**Table S10.** Device performance of PM6-b-PYIT devices incorporating different Y6 amounts and N-DMBI dopants under the illumination of AM 1.5G, 100 mW $cm^{-2}$. [a]

| Condition | $V_{OC}$ (V) | $J_{SC}$ (mA/$cm^2$) | FF (%) | PCE (%) |
|---|---|---|---|---|
| PM6-b-PYIT +1%Y6 | 0.931 (0.928±0.001) | 23.6 (23.3±0.2) | 66.0 (64.6±1.0) | 14.5 (14.2±0.2) |
| PM6-b-PYIT +1%Y6+0.01%wt N-DMBI | 0.931 (0.930±0.001) | 23.4 (23.2±0.2) | 66.6 (64.9±0.9) | 14.6 (14.3±0.2) |
| PM6-b-PYIT +1%Y6+0.05%wt N-DMBI | 0.931 (0.929±0.002) | 24.0 (23.8±0.1) | 65.4 (64.7±0.4) | 14.6 (15.3±0.2) |
| PM6-b-PYIT +1%Y6+0.1%wt N-DMBI | 0.931 (0.930±0.001) | 24.4 (24.2±0.2) | 66.0 (65.0±0.5) | 15.0 (14.8±0.2) |
| PM6-b-PYIT +3%Y6 | 0.931 (0.928±0.002) | 23.8 (23.7±0.1) | 66.4 (65.6±0.4) | 14.7 (14.5±0.1) |
| PM6-b-PYIT +3%Y6+0.01%wt N-DMBI | 0.936 (0.933±0.002) | 23.7 (23.53±0.1) | 67.6 (67.1±0.3) | 15.0 (14.8±0.10) |
| PM6-b-PYIT +3%Y6+0.05%wt N-DMBI | 0.944 (0.943±0.001) | 24.6 (24.2±0.3) | 68.5 (68.2±0.2) | 15.9 (15.5±0.3) |
| PM6-b-PYIT +3%Y6+0.1%wt N-DMBI | 0.938 (0.936±0.002) | 23.9 (23.8±0.2) | 67.5 (66.6±0.6) | 15.1 (14.8±0.3) |
| PM6-b-PYIT +5%Y6 | 0.931 (0.930±0.001) | 23.3 (23.1±0.2) | 63.3 (63.2±0.8) | 13.7 (13.6±0.1) |
| PM6-b-PYIT +5%Y6+0.01%wt N-DMBI | 0.931 (0.930±0.001) | 23.9 (23.6±0.2) | 63.0 (62.5±0.4) | 14.0 (13.8±0.2) |

[a] The parameters are obtained from 10 independent devices.

**Table S11.** The *n* values obtained from fitting the $V_{OC}$-$P_{light}$ curves.

| | PM6-b-PYIT | PM6-b-PYIT doped | PM6-b-PYIT+Y6 | PM6-b-PYIT+Y6 +N-DMBI |
|---|---|---|---|---|
| ***α* value** | 0.982±0.002 | 0.983±0.002 | 0.989±0.001 | 0.993±0.003 |
| ***n* values** | 1.52±0.03 *k*T/q | 1.51±0.04 *k*T/q | 1.44±0.02 *k*T/q | 1.25±0.03 *k*T/q |

**Table S12.** Performances of devices based on blends of PM6-b-PYIT with BTP-eC9 or L8-BO and doped by N-DMBI under the illumination of AM 1.5G, 100 mW $cm^{-2}$. [a]

| Active layer | $V_{OC}$ (V) | $J_{SC}$ (mA/$cm^2$) | FF (%) | PCE (%) |
|---|---|---|---|---|
| PM6-b-PYIT +3%BTP-eC9 | 0.931 (0.930±0.001) | 23.5 (23.2±0.3) | 67.3 (67.1±0.2) | 14.7 (14.6±0.1) |
| PM6-b-PYIT +5%BTP-eC9+0.05%wt N-DMBI | 0.939 (0.938±0.001) | 23.5 (23.3±0.1) | 69.1 (68.6±0.4) | 15.2 (15.1±0.1) |
| PM6-b-PYIT +3%L8-BO | 0.933 (0.932±0.001) | 24.2 (23.8±0.3) | 65.7 (64.9±0.5) | 14.8 (14.5±0.2) |
| PM6-b-PYIT +5%L8-BO+0.05%wt N-DMBI | 0.938 (0.937±0.001) | 24.0 (23.8±0.1) | 69.0 (68.3±0.5) | 15.5 (15.4±0.1) |

[a] The parameters were obtained over 10 independent devices.

**Table S13.** Optimized XGBoost model hyperparameters.

| Hyperparameter | Purpose of the Hyperparameter | Value |
|---|---|---|
| n_estimators | Number of decision trees | 100 |
| max_depth | Depth of the tree | 3 |
| learning_rate | Learning rate | 0.05 |
| subsample | Sample Sampling Ratio | 0.5 |

**Table S14.** Normalized photovoltaic parameters of PM6-b-PYIT OSCs in nitrogen atmosphere for up to 1000 h storage under 85°C continuous annealing under dark condition. [a]

| Time (h) | $V_{OC}$ (V) | Er± | $J_{SC}$ (mA cm$^{-2}$) | Er± | FF (%) | Er± | PCE (%) | Er± |
|---|---|---|---|---|---|---|---|---|
| 0 | 1.000 | 0.005 | 1.000 | 0.026 | 1.000 | 0.020 | 1.000 | 0.036 |
| 6 | 0.998 | 0.002 | 0.999 | 0.018 | 0.961 | 0.010 | 0.877 | 0.011 |
| 18 | 0.989 | 0.002 | 0.989 | 0.017 | 0.938 | 0.017 | 0.829 | 0.030 |
| 40 | 0.986 | 0.003 | 0.975 | 0.013 | 0.925 | 0.020 | 0.812 | 0.026 |
| 52 | 0.987 | 0.001 | 0.951 | 0.009 | 0.915 | 0.011 | 0.813 | 0.014 |
| 64 | 0.983 | 0.003 | 0.937 | 0.023 | 0.902 | 0.017 | 0.807 | 0.031 |
| 88 | 0.975 | 0.001 | 0.929 | 0.015 | 0.901 | 0.013 | 0.763 | 0.024 |
| 112 | 0.976 | 0.009 | 0.903 | 0.017 | 0.886 | 0.022 | 0.739 | 0.017 |
| 144 | 0.974 | 0.007 | 0.896 | 0.023 | 0.893 | 0.007 | 0.735 | 0.021 |
| 176 | 0.974 | 0.012 | 0.859 | 0.033 | 0.886 | 0.013 | 0.706 | 0.027 |
| 240 | 0.976 | 0.013 | 0.876 | 0.025 | 0.885 | 0.013 | 0.718 | 0.022 |
| 312 | 0.974 | 0.017 | 0.856 | 0.028 | 0.876 | 0.013 | 0.708 | 0.032 |
| 420 | 0.976 | 0.003 | 0.843 | 0.015 | 0.863 | 0.022 | 0.725 | 0.021 |
| 600 | 0.974 | 0.001 | 0.841 | 0.017 | 0.854 | 0.013 | 0.706 | 0.027 |
| 800 | 0.972 | 0.009 | 0.835 | 0.023 | 0.850 | 0.022 | 0.718 | 0.022 |
| 1000 | 0.970 | 0.007 | 0.833 | 0.033 | 0.846 | 0.007 | 0.708 | 0.032 |

[a] The parameters are obtained from 5 independent devices.

**Table S15.** Normalized photovoltaic parameters of PM6-b-PYIT+3%Y6 OSCs in nitrogen atmosphere for up to 1000 h storage under 85°C continuous annealing under dark condition. [a]

| Time (h) | $V_{OC}$ (V) | Er± | $J_{SC}$ (mA cm$^{-2}$) | Er± | FF (%) | Er± | PCE (%) | Er± |
|---|---|---|---|---|---|---|---|---|
| 0 | 1.000 | 0.003 | 1.000 | 0.008 | 1.000 | 0.012 | 1.000 | 0.020 |
| 6 | 0.995 | 0.002 | 0.985 | 0.006 | 0.970 | 0.008 | 0.923 | 0.012 |
| 18 | 0.991 | 0.002 | 0.979 | 0.014 | 0.953 | 0.009 | 0.889 | 0.012 |
| 40 | 0.989 | 0.004 | 0.951 | 0.029 | 0.944 | 0.002 | 0.872 | 0.027 |
| 52 | 0.980 | 0.002 | 0.933 | 0.017 | 0.934 | 0.004 | 0.850 | 0.014 |
| 64 | 0.981 | 0.004 | 0.933 | 0.023 | 0.923 | 0.005 | 0.807 | 0.019 |
| 88 | 0.977 | 0.002 | 0.933 | 0.021 | 0.902 | 0.006 | 0.820 | 0.015 |
| 112 | 0.978 | 0.010 | 0.926 | 0.026 | 0.913 | 0.006 | 0.796 | 0.026 |
| 144 | 0.973 | 0.008 | 0.897 | 0.022 | 0.903 | 0.011 | 0.788 | 0.026 |
| 176 | 0.975 | 0.009 | 0.905 | 0.020 | 0.896 | 0.008 | 0.781 | 0.025 |
| 240 | 0.973 | 0.010 | 0.914 | 0.015 | 0.901 | 0.027 | 0.776 | 0.028 |
| 312 | 0.974 | 0.018 | 0.893 | 0.017 | 0.895 | 0.024 | 0.755 | 0.026 |
| 420 | 0.973 | 0.002 | 0.887 | 0.014 | 0.890 | 0.011 | 0.768 | 0.026 |
| 600 | 0.975 | 0.010 | 0.885 | 0.029 | 0.886 | 0.008 | 0.761 | 0.025 |
| 800 | 0.973 | 0.008 | 0.871 | 0.017 | 0.874 | 0.027 | 0.756 | 0.028 |
| 1000 | 0.970 | 0.009 | 0.869 | 0.023 | 0.873 | 0.024 | 0.745 | 0.026 |

[a] The parameters are obtained from 5 independent devices.

**Table S16.** Normalized photovoltaic parameters of PM6-b-PYIT+3%Y6 doped OSCs in nitrogen atmosphere for up to 1000 h storage under 85°C continuous annealing under dark condition. [a]

| Time (h) | $V_{OC}$ (V) | Er± | $J_{SC}$ (mA cm$^{-2}$) | Er± | FF (%) | Er± | PCE (%) | Er± |
|---|---|---|---|---|---|---|---|---|
| 0 | 1.000 | 0.003 | 1.000 | 0.017 | 1.000 | 0.020 | 1.000 | 0.033 |
| 6 | 0.998 | 0.003 | 0.992 | 0.010 | 0.965 | 0.016 | 0.940 | 0.023 |
| 18 | 0.994 | 0.003 | 0.989 | 0.014 | 0.960 | 0.024 | 0.900 | 0.036 |
| 40 | 0.991 | 0.003 | 0.978 | 0.014 | 0.945 | 0.017 | 0.885 | 0.026 |
| 52 | 0.990 | 0.004 | 0.985 | 0.018 | 0.941 | 0.012 | 0.878 | 0.026 |
| 64 | 0.985 | 0.003 | 0.980 | 0.022 | 0.937 | 0.005 | 0.882 | 0.025 |
| 88 | 0.981 | 0.004 | 0.973 | 0.019 | 0.935 | 0.012 | 0.873 | 0.026 |
| 112 | 0.979 | 0.001 | 0.981 | 0.006 | 0.937 | 0.007 | 0.886 | 0.011 |
| 144 | 0.979 | 0.002 | 0.961 | 0.017 | 0.942 | 0.013 | 0.859 | 0.006 |
| 176 | 0.977 | 0.004 | 0.962 | 0.019 | 0.935 | 0.007 | 0.855 | 0.019 |
| 240 | 0.974 | 0.007 | 0.963 | 0.017 | 0.936 | 0.010 | 0.851 | 0.023 |
| 312 | 0.972 | 0.008 | 0.954 | 0.019 | 0.929 | 0.036 | 0.843 | 0.023 |
| 420 | 0.981 | 0.004 | 0.931 | 0.019 | 0.916 | 0.013 | 0.849 | 0.026 |
| 600 | 0.979 | 0.003 | 0.935 | 0.006 | 0.913 | 0.007 | 0.845 | 0.026 |
| 800 | 0.979 | 0.004 | 0.923 | 0.017 | 0.906 | 0.010 | 0.840 | 0.025 |
| 1000 | 0.977 | 0.001 | 0.921 | 0.019 | 0.903 | 0.036 | 0.833 | 0.026 |

[a] The parameters are obtained from 5 independent devices.

## 4. Supplemental Reference


1. A. Hexemer, W. Bras, J. Glossinger, E. Schaible, E. Gann, R. Kirian, A. MacDowell, M. Church, B. Rude and H. Padmore, *J. Phys.: Conference Series*, 2010, **247**, 012007.
2. F. Neese, *WIREs Comput. Molecular Sci*., 2022, **12**, 1606.
3. F. Neese, F. Wennmohs, U. Becker and C. Riplinger, *J. Chem. Phys.*, 2020, **152**, 224108.
4. T. Lu and F. Chen, *J. Comput. Chem.*, 2012, **33**, 580-592.